Project Description

Introduction: semiconductor scintillator. There are two large groups of solid-state radiation detectors, which dominate the area of ionizing radiation measurements, scintillation detectors and semiconductor diodes. The scintillators detect high-energy radiation through generation of light which is subsequently registered by a photo-detector that converts light into an electrical signal. The main advantage of existing scintillators is their low cost and large detection volume. Semiconductor diodes employ reverse biased junctions where the absorbed radiation creates electrons and holes, which are separated by the junction field thereby producing a direct electrical response. The sensitivity of diode detectors depends on the length of the field region and requires high-purity materials. At present, the semiconductor diode is best for the spectral resolution of the ionizing radiation.

As reviewed extensively by Knoll [1], both groups of detectors have their drawbacks, resulting in a lower than desired signal response and resolution. The diodes typically suffer from inadequate electron-hole collection, i.e. not every electron-hole pair created by the radiation results in a current flow in the measurement circuit. The most common semiconductor materials used for the radiation detectors are Si and Ge p-n junctions, where the intrinsic carrier concentration can be reduced to a very low level, while the excellent material properties provide for good electric field uniformity. Both Si and Ge radiation detectors require relatively high voltages, typically of order kilovolts, to maximize the collection of electrons and holes and increase their drift velocity. Even at these high voltages, the response time is larger than 100 ns, limited by the saturated electron and hole drift velocities at high fields.

In the case of scintillators, the efficiency of converting the high-energy radiation into light is typically about 10% (12% in NaI). The reason for this is fundamental: the scintillator material must be transparent to the radiation it produces. To accomplish this, the wide-gap material (7 eV for NaI) is activated with impurities such as thallium which represent recombination sites for electrons and holes. Thus produced light has much lower energy (3 eV for Tl) than the bandgap of the host crystal, whence the poor absolute efficiency. The poor efficiency translates into low energy resolution in scintillators. In addition, the recombination time is several hundreds of nanoseconds (e.g., 230 ns for NaI activated with Tl), which is undesirably long for fast timing or high counting rate applications. Finally, the high bandgap inherent in all commercially available scintillators implies a relatively high energy (25 eV for NaI) required per each electron-hole pair created by the ionizing radiation. This also reduces the detector resolution.

Recently we proposed [2,3] a new scintillation-type semiconductor detector in which high-energy radiation produces electron-hole pairs in a direct-gap semiconductor material that subsequently undergo *interband recombination,* producing infrared light to be registered by a photo-detector. The key issue is how to make the semiconductor essentially transparent to its own infrared light, so that photons generated deep inside the semiconductor slab could reach its surface without tangible attenuation. We proposed a novel way to accomplish this, based on doping the semiconductor with shallow donors to produce the Burstein shift between emission and absorption spectra.

The device is contemplated for the implementation in compound semiconductor materials, such as GaAs or InP, where a mature optoelectronic technology exists. This enables a novel

system architecture, where each relatively thin semiconductor slab (e.g., standard 0.5 mm-thick wafer) is supplied with its own, epitaxially grown or grafted on the surface, photo-detector system. Such systems can then be stacked up without limit, thus increasing the active detector volume to accommodate large absorption length of high-energy radiation – without any loss in scintillator yield and speed of response.

The most innovative feature of the proposed detector is that it enables three-dimensional integration [4] of standard semiconductor wafers, each provided with a pixellated epitaxial photosensitive layer on its surface as well as amplifying and analog-to-digital electronic circuits. The information about each ionizing radiation event, comprising simultaneous response from several three-dimensional (3D) pixels, is converted to digital form, suitable for rapid analysis. The 3D pixellation of the scintillator response enables *both* accurate determination of incident particle energy *and* high-resolution angular discrimination. This goes to the heart of the homeland security needs, where accurate spectral characterization is of the essence to avoid "false alarms". Our proposed technology offers unprecedented fidelity in isotope discrimination. The integrated device, functionally a monolithic 3D scintillator array of linear dimensions limited only by the size of a semiconductor wafer, will have the spectroscopic resolution of best semiconductor diodes and provide an accurate determination of the direction to source at the same time. Both advantages are to be realized simultaneously in a compact relatively inexpensive detector manufacturable by the mature methods of modern microelectronics.

1. Physical principle: Scintillator based on Burstein shift. When semiconductor is heavily doped, the edge of absorption is blue-shifted relative to the emission edge by the carrier Fermi energy. This quantum effect, illustrated in Fig. 1, is called the Burstein shift. It underlies operation of all semiconductor lasers. The absorption mean free path $\lambda = \lambda_0 \exp(E_F / kT)$ increases exponentially with the Fermi level E_F (where λ_0 is the absorption mean free path in the undoped material, $\lambda_0 \approx 1\,\mu m$ in InP).

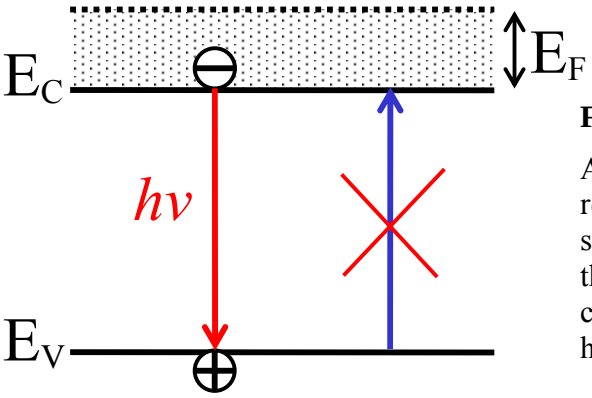

Figure 1. Illustration of Burstein shift

Absorption of photons $h\nu$, emitted by recombining electrons and hole in the semiconductor, is largely suppressed by the absence of vacant electron states in the conduction band under the Fermi level in heavily doped semiconductor.

Besides making the semiconductor transparent to its own emitted photons, the heavy doping shortens the radiative recombination time τ of minority carriers, according to $\tau = 1/BN_D$, where $B=10^{-10}$ cm^3/s is the radiative recombination coefficient. For the donor concentration $N_D = 10^{19}$ cm^{-3} in InP, one has $\tau \sim 10^{-9}$s. The non-radiative time in this range of concentrations is limited by Auger recombination and is of order $\sim 10^{-7}$s. Therefore, the

ratio ξ of the radiative and non-radiative recombination time is ξ~0.01. Thus, the device experiences practically no losses through the non-radiative channels of recombination.

For N_D =10^{19} cm^{-3}, the ratio E_F/kT ~ 8 in InP at room temperature, thus yielding the absorption mean free path $\lambda \approx 3\,\mathrm{mm}$. Further increase of the doping, desirable for the increase of the E_F/kT ratio, becomes impractical due to the rise of the *free-carrier absorption* (FCA), limiting λ to about 1 mm at room temperature, which is still larger than the standard thickness of an InP wafer. The FCA coefficient in semiconductors is not a universal parameter because absorption of photons by free electrons is forbidden by the conservation of momentum and energy and thus essentially depends on a third agent, impurity or phonon. The FCA in InP was studied by Dumke and coworkers [5]. It turns out that for photon energies below but near the fundamental bandgap (the region we are interested in) the dominant absorption process is due to free-carrier transitions to higher-lying conduction-band valleys. For the free-carrier concentration of 10^{19} cm^{-3} in InP, the absorption coefficient is about 7 to 10 cm^{-1}, corresponding to $\lambda \approx 1$ mm. The measured free-carrier absorption coefficient scales rather accurately with the carrier concentration. Recent accurate study of FCA in GaAs and InGaAsP on InP was reported by Reinhart [6].

It is clear that to operate our detector we must keep the device thickness below the free-carrier absorption length. We are planning, therefore, to use standard InP wafers of thickness under 0.5 mm and doping approaching 10^{19} cm^{-3}. One of our important initial tasks is to find the optimum doping concentration to ensure the highest optical output in the wavelength range corresponding to the InP fundamental emission spectrum. In our preliminary optical experiments with InP doped with S to $N_D \approx 6\times10^{18}$ cm^{-3}, the integrated luminescence intensity measured in the transmission geometry – in response to photoexcitation from one side of the wafer – was about 50% of that measured in the reflection geometry at room temperature and over 70% at 77K. This indicates that the doped wafer is indeed largely transparent to its own interband radiation.

In the context of the present proposal, we shall study the Burstein shift in InP and GaAs, as functions of temperature and the concentration of *different* shallow impurities. Although the effect is supposed to be universal, its effectiveness depends on the material quality.

2. Epitaxial photoreceiver and stacking of InP slabs. It is clear that the thickness of an InP scintillator slab must be less than the attenuation length of the scintillating radiation. As discussed in the preceding section, this attenuation length is limited by the lesser of the mean free paths of scintillating photons against (a) interband absorption and (b) the free-carrier absorption. At room temperature, the expected attenuation length is 1 mm and therefore the wafer thickness of 0.5 mm (standard in optoelectronics) is acceptable. The bandgap of undoped InP at 300K is $E_G = 1.35\,\mathrm{eV}$. In heavily doped semiconductors the gap is known to shrink a little and one of our tasks is to quantify this shrinkage accurately. This is to be accomplished by measuring the luminescence spectrum in our samples. The next step is to design the appropriate photoreceiver material, to be grown epitaxially on InP. The photoreceiver bandgap must be lower than that of doped InP, so that the entire luminescence spectrum is absorbed. On the other hand, it should not be narrower than necessary, because for narrower gaps, the photoreceiver noise increases due to thermal leakage current. From our experience, the first design will shoot for the photoreceiver

bandgap $E_G^{\mathrm{Ph}} = 1.24\,\mathrm{eV}$. The epitaxial photoreceiver will be implemented as a quaternary $In_{1-x}Ga_xAs_yP_{1-y}$ alloy lattice-matched to InP. The lattice-matched heterostructure is important because otherwise dislocations will have a detrimental effect on the photoreceiver performance. For lattice-matched compositions ($x = 0.454y$) the alloy bandgap is given by [7] $E_G(y) = 1.35 - 0.72y + 0.12y^2$, so that the desired value is achieved with $x = 0.07,\ y = 0.16$. The epitaxial structure is illustrated in Fig. 2.

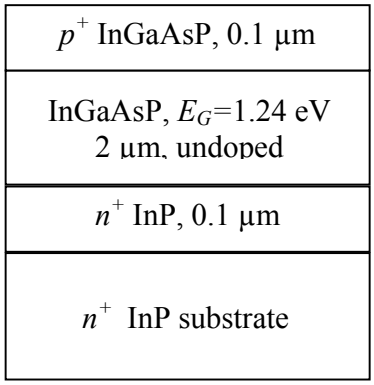

Figure 2. Schematic diagram of the proposed epitaxial *pin* photodetector lattice-matched to InP.

The critical region is the nominally undoped 2μm thick active region of the diode. It must be sufficiently pure for the entire region to be depleted by an applied bias of less than 5 V.

The structure will be grown by MBE and MOCVD on a commercial basis.

Once the InP scintillator slabs are endowed with an efficient epitaxial photodetector, they can be stacked, essentially without limit. Each layer in the stack is a pixel in z direction. Pixellation in *xy* direction is accomplished by processing the epitaxial layer into a photodiode array. Electrical signals from each individual detector slab are electronically processed in each slab and converted to a digital information. In this case, every slab in the stack represents an opto-electronic chip, delivering the information in a digital, noise-free format. We emphasize that each integrated chip reports not a short analog pulse, but a digital signal carrying the required information – where in the stack the photo-multiplication occurred, the time of the event, its amplitude, and the lateral coordinates of the event. Such an integrated system offers enormous advantages for definite error-free identification and characterization of high-energy radiation, as well as accurate determination of the direction to source.

The lateral dimension of a pixel must be larger than the slab thickness, so that light produced by each individual interaction event is registered by one pixel only. The number of pixels $m \times n$ in each slab is therefore about 100 per cm^2 and for large chip area (several square inches) we should be concerned that the number of data lines and data converters scale as $m + n$, not as $m \times n$. Having in mind this scaling consideration, we shall design the photo detection matrix with the requisite mixed-signal ASIC's (application-specific integrated circuits) and have the latter fabricated commercially at a silicon foundry. The design is rather non-trivial because of the large capacitance associated with an individual pixel and the short duration of the current pulse associated with a single interaction event.

3. InP versus GaAs. Different considerations favor either of these two semiconductors. The most important consideration is *cost*: GaAs is cheaper and is associated with a relatively more mature electronics technology. The fact that indium has a relatively high atomic number (Z=49) favors InP from the standpoint of photoelectric absorption, but Compton

scattering processes in InP and GaAs are similar because both materials have the same total Z per unit cell of the crystal. GaAs has a lower effective electron mass and therefore lower effective density of states in the conduction band ($4.7\cdot10^{17}$ versus $5.7\cdot10^{17}$ cm^{-3} in InP). This means that the same Burstein shift and interband absorption suppression can be obtained in GaAs with lower doping and hence lower free-carrier absorption. Another advantage of GaAs is its higher ratio of radiative to nonradiative recombination. Furthermore, the most important advantage of GaAs from the technical standpoint, is that GaAs has a higher bandgap than InP ($E_G = 1.42$ eV versus 1.35 eV). This translates into the potential for higher photodetector bandgap ($E_G^{\mathrm{Ph}} = 1.32$ eV versus 1.24 eV in Fig. 2) and therefore lower dark current at room temperature.

Still, we regard GaAs approach as substantially higher risk. The problem lies in the absence of a proven epitaxial detector material. Standard heterostructures lattice-matched to GaAs (notably $Al_xGa_{1-x}As$) have a *higher* bandgap, whereas we need lower. We propose a high-risk approach based on *dilute nitride* technology [8]. Due to its high electronegativity and small size, nitrogen dramatically reduces the bandgap of III-V compound semiconductors when added in small amount (atomic percent). It also shrinks the lattice constant and so to remain lattice-matched to GaAs one needs to compensate for the strain by incorporating some indium. The exact lattice-matched composition of $In_xGa_{1-x}As-N_y$ that will provide $E_G^{\mathrm{Ph}} = 1.32$ eV, needs special research and whether or not the material can be made pure enough (background less than 10^{16} cm^{-3}) is unknown. This approach will be investigated in collaboration with Rachel Goldman of the University of Michigan, who has demonstrated [9] record electronic quality dilute-nitride GaAs-N layers by MBE. The epitaxial detector structure will be similar to that in Fig. 2 with GaAs instead of InP and with the dilute-nitride InGaAs-N ($E_G = 1.32$ eV) replacing the quaternary active detector layers. The risk is mitigated by the parallel track of proven InGaAsP technology lattice-matched to InP.

4. Advantages of 3D pixellation. Breaking down the ionizing interaction into events, resolved both in space and in energy, is well known to offer a dramatically higher information content, compared to measuring only the total energy deposited by the ionizing particle[10]. A large body of research exists to use this enhanced information in the so-called Compton telescopes, see e.g. Kurfess et al.[11], and Boggs and Jean[12].

An incident γ photon of energy E_0 and direction $\hat{n}_0$ undergoes Compton scattering at an angle θ_1 and deposits an energy L_1 in the electronic system at the position $\vec{r}_1$ within the detector. The scattered photon travels in the direction $\hat{n}_1$, suffers another Compton scattering at $\vec{r}_2$, depositing there an energy L_2, and so on until it is eventually photoabsorbed. A 3D pixellated detector such as ours measures a cluster of several points $\{\vec{r}_i, L_i\}$ for each incident photon. All points in the cluster appear essentially simultaneously upon the arrival of a γ photon. Nevertheless, there exist powerful techniques to assign a correct order to the cluster points. These techniques, originated by Aprile et al. [13], are primarily based on the kinematics of Compton scattering, expressed by the following equation (where all energies are expressed in units of the electron rest energy, $m_e c^2 = 511$ keV):

$$\cos\theta_i = 1 + E_{i-1}^{-1} - E_i^{-1}$$
$$L_i = E_{i-1} - E_i \qquad (1)$$

With three points $\{\vec{r}_i, L_i\}$ $(i = 1, 2, 3)$ measured and identified in the correct order, one knows θ_2 and has four equations in 4 unknowns: θ_1, E_0, E_1, E_2. This means that one can determine the incident energy E_0 irrespectively of whether the cluster comprises all deposited energies, cf. Fig. 3.

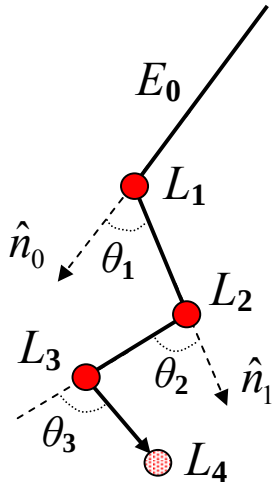

Figure 3. Illustration of the Compton telescope concept. With first three interactions identified in the correct order, equations (1) yield the energy E_0 of the incident photon in terms of the measured energies of two interactions, L_1 and L_2, and the direction $\cos\theta_2$ of the second Compton scatter:

$$E_0 = L_1 + \frac{L_2}{2} + \frac{1}{2}\left(L_2^2 + \frac{4L_2}{1-\cos\theta_2}\right)$$

The order of interactions is determined probabilistically, based on the scattering cross-section (2) and additional kinematic information from the position of L_4.

One also finds some information about the direction to the source, namely the angle θ_1 about the measured direction $\hat{n}_1$, viz. $\cos\theta_1 = 1 + E_0^{-1} - E_1^{-1}$. The point source is thus placed on a cone. After two γ photons are received, the direction is uniquely specified.

The technique works to the extent that one can order the events. Measurement of a fourth point $\{\vec{r}_4, L_4\}$ in the cluster adds two equations and only one unknown and therefore can be used to determine the correct sequence. If all the measured quantities $\{\vec{r}_i, L_i\}$ had a mathematical precision, the system of equations would be consistent only for the correct order. In practice, because both the positions and energies $\{\vec{r}_i, L_i\}$ are measured only to within a certain margin of accuracy, the determination of the best order (a.k.a. tracking algorithm or event reconstruction) becomes a statistical procedure that minimizes inconsistency. Current tracking algorithms claim up to 70% success in correctly ordering events produced by a 1 MeV photon. To further improve the ordering procedure, the probabilistic analysis can include, besides the Compton kinematics, the anisotropic scattering cross-sections $\sigma(\theta_i)$, expressed by the well-known Klein-Nishina formula.

Compared to the existing Compton telescopes, the 3D–pixellated device we propose has multiple advantages from the standpoint of DNDO applications. These advantages are reminiscent of those brought to electronics by the advent of integrated circuits. The Compton telescopes are built as an assembly of discrete detectors, usually Ge diodes. Besides the obvious advantage of the compact size and low cost, our device offers an

enormous increase in the pixel density, which ultimately translates into the better resolution. An inch-sized cubic device will comprise about $3 \cdot 10^4$ pixels forming 1 mm pitch arrays in *xy* planes and 0.5 mm pitched stack in the *z* direction. Another unique advantage of our device is its high-speed of response, limited only by the radiative recombination time of about 1 ns. This means that in practical situations of interest to DNDO we shall be always looking at one cluster at a time. Our preliminary estimates suggest that for 660 keV photons we should be able to determine the energy with an accuracy in the range of 1 to 3 keV, corresponding to an energy resolution better than 0.5%. Our 3D-integrated scintillator will have the isotope discrimination power similar to that of the best semiconductor diodes.

At the same time, we shall resolve the direction to a point source. The Compton telescope procedure, described by Eqs. (1) and illustrated in Fig. 3, yields the directional cosine about the measured direction $\hat{n}_1$ which means the object is placed on a cone about $\hat{n}_1$. Repeated measurements for three clusters produce cones about varied $\hat{n}_1$ and this allows to determine the azimuth angle as well. It may be worth noting that the problem of resolving the direction to a point source is different from the precision of imaging (e.g., from resolving two point sources at a close distance). Thus the angular resolution in Compton telescope imaging cannot be better than a few degrees, as limited by the Doppler effect. However, this does not limit the precision of finding the direction to the point source.

In the context of the present proposal, we shall develop novel electronic circuits and signal processing — optimized for 3D matrix readout. Available 2D solutions are not sufficient in the long-run, having in mind a highly pixellated detector with multiple layers in the stack.

5. General advantages of a direct-gap semiconductor scintillator. As discussed above, we regard as the main advantage of the proposed semiconductor scintillator the fact that it naturally lends itself to the very advantageous 3D integration. It is also worth reviewing the general advantages of using direct-gap semiconductors, such as InP and GaAs, as a scintillator material. The direct-gap scintillator has a high detection efficiency and a response time in the nanosecond range. The relatively low energy gap, and therefore low energy per single photon (about 4 eV for either InP or GaAs versus 25 eV for NaI) gives the absolute photon yield of ~ 250,000 photons/MeV, versus ~ 40,000 photons/MeV for NaI. It is instructive to compare the absolute scintillator efficiencies, defined as $\eta = \left(E_\gamma / 3E_G\right) \times \left(h\nu / E_\gamma\right)$, where E_γ is the particle energy, $3E_G$ the average energy to create an electron-hole pair, and $h\nu$ the energy of scintillating photons. In thallium-activated NaI electron-hole pairs are produced across the band-gap of over 7 eV while the scintillating photons are produced at *hν* of only 3 eV, whence the best η available in NaI scintillators is about 12%. In contrast, the effective value of $3E_G$ in both InP and GaAs is 4.1 eV and the *hν* of scintillating photons is close to E_G. We can expect therefore an improvement in η by a factor of 7/3 over thallium-activated NaI. This estimate does not include well-known additional losses at the photomultiplier, which typically has less than 25% light-to-current conversion efficiency. Our device with epitaxial photosensors offers nearly 100% conversion efficiency. GaAs diodes have been used as high energy resolution (Fano factor $F = 0.12 \pm 0.01$) radiation detectors [14]. GaAs scintillator can be expected to have a similar resolution.

Our device does not need high voltages or low temperatures for operation and is robust against the hostile environment, e.g. it can operate in high magnetic fields.[1] Among the many attractive features of the proposed detector, we should single out its exceptionally fast response. We note that the prompt response of our detector is *not* owing to the quenching of the radiative transitions by non-radiative processes and, therefore, is not accompanied by any degradation of brightness. Our fast response is based on the fact that radiative transitions are themselves fast in a direct-gap semiconductor at a sufficiently high majority-carrier concentration. This property has not been utilized before in a high-energy radiation detector because fast transition rates are normally associated with short mean-free path of the resultant scintillating radiation. *Breaking this association is the essence of our invention.* Our detector is simultaneously fast and bright.

6. Heterostructure Scintillator. As discussed in Sect. A1, the uniform scintillator, based on the Burstein shift, is limited by the combination of interband and free-carrier absorption to a thickness of about 1 mm at room temperature. Let us now discuss a modified structure, where the problem of absorption *is largely eliminated,* Fig. 4.

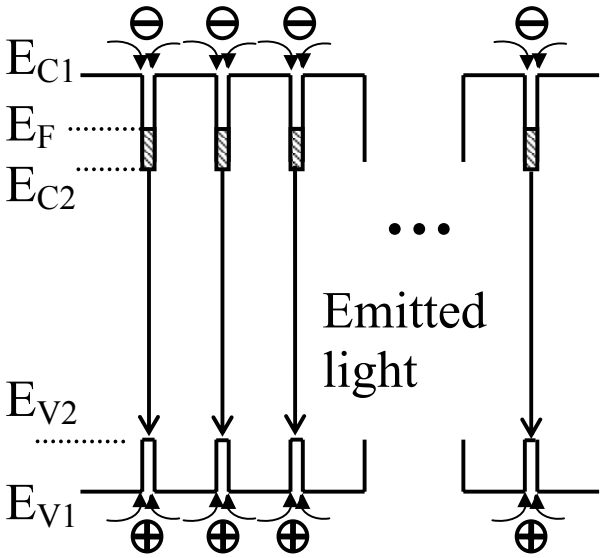

Figure 4. Heterostructure detector based on bandgap engineering.

The heterostructure comprises two alternating materials, e.g., InP and InGaAsP quaternary alloy, lattice matched to InP, forming narrow wells, doped with donor impurities. Spacing between the wells, about 2 μm, is much larger than the well thickness.

Electrons and holes generated by the ionizing radiation rapidly diffuse to the wells and recombine there, producing scintillating radiation to which the heterostructure material is transparent.

The epitaxial structure comprises two alternating materials lattice-matched to each other. The materials are assumed to have different energy gap, respectively $E_{G1} = E_{C1} - E_{V1}$ and $E_{G2} = E_{C2} - E_{V2}$, with the second material having the lower bandgap, $E_{G1} > E_{G2}$. We further assume the second material is doped, while the first material is largely undoped.

The essential idea [2, 3] is that the total volume occupied by the second material is small compared to that occupied by the first material. For example, if a 2μm-thick InP layers are alternated by a 20 nm-thick layers of InGaAsP, the layer thickness ratio is 100 (duty cycle factor δ=0.01). Upon interaction with the ionizing radiation, the created electrons and holes quickly, within about a nanosecond, diffuse to the wells and recombine there. The

[1] The scintillator itself requires no electrical bias. Small voltage must be applied to operate an integrated detector of light produced by the scintillator.

difference in the band-gap energies (1.35eV for InP and 1.2 eV for InGaAsP) guarantees that all light emission occurs in the InGaAs wells, so that the wider-gap InP remains substantially transparent to the emitted photons.

It should be emphasized that the Burstein shift remains important for the viability of the heterostructure detector. The recombination wells can be viewed as artificial "giant traps" for electrons and holes, which act essentially as efficient radiative recombination centers without introducing non-radiative recombination. Without the Burstein shift, the efficient radiative recombination would translate into equally efficient absorption.

With interband self-absorption suppressed by the Burstein shift, the only remaining absorption in the heterostructure is owing to free carriers in the wells. However, the effective FCA coefficient is reduced by the duty cycle factor. With the doping density in the wells $N_D=10^{19}$ cm^{-3} and $\delta=0.01$, we obtain the total absorption coefficient of less than 0.1 cm^{-1}. Thus, the active material in the heterostructure detector is practically transparent to the emitted light at room temperature and the collection efficiency approaches unity. High electron density in the narrow-gap wells guarantees both that the radiation recombination is a dominant process and that the response time is about 1 nanosecond.

Needless to say, the fabrication of this device is not simple. Indeed, most epitaxial growth techniques capable of nano-resolution, such as the metalorganic vapor phase epitaxy (MOCVD), are associated with a relatively slow growth process. The challenge is entirely in the growth time that may span several days, but because of the superior material quality produced with MOCVD, it may be still preferred and used advantageously. The other preferred method is the hydride vapor phase epitaxy, HVPE, which allows a growth rate of 100 μm per hour and even higher. At this time HVPE is primarily used for growing free standing GaN structures [15]. The free-standing epitaxial 500 μm-thick films can be grown on a thin substrate that is subsequently removed.

This is an extremely high-risk approach that nevertheless must be tried because the payout is so high. We intend to test several approaches — all on the commercial basis — including MOCVD, HVPE, and perhaps even liquid-phase epitaxy (LPE).

7. Theoretical studies of the statistics; variance and the Fano factor. Energy resolution of a gamma detector relies on the ability to evaluate the energy deposited in Compton and photoelectric events. As high-energy particle propagates through a semiconductor, it multiplies producing secondary electron-hole (e-h) pairs. The measured quantity is the number N of e-h pairs produced in the course of particle energy branching (PEB). This number is estimated through integrating the current pulse in *pin* diode-detectors or via the number of low-energy photons generated in scintillators by absorption of gamma quantum. Variance of this number, due to the random character of energy branching and also due to random energy losses in phonon emission, limits the accuracy of energy measurements.

Both the yield N and its variance $\mathrm{var}(N)=\overline{\left(N-\overline{N}\right)^2}$ are proportional to the initial energy. The ratio $F=\mathrm{var}(N)/N$, called the Fano factor of the PEB process, is a parameter that quantifies energy resolution. If the statistics of PEB were Poisson, one would have $F=1$. As it turns out, the Fano factor can be rather small in semiconductors, $F=0.1$ and even smaller, which means that the PEB is a highly correlated process [16].

The problem of PEB statistics is mathematically similar to a model problem of random sequential adsorption (RSA). The simplest embodiment of RSA is called the car parking problem or CPP, where one studies the average number of particles ("cars") adsorbed on a long line and the variance of this number. The affinity between the two problems was fully recognized already in 1965 by van Roosbroek [17] (see also [18]). The PEB process can be considered in terms of a CPP if one identifies the initial particle kinetic energy with an available parking length and the pair creation energy with the car size.

All reported attempts to evaluate *F* employed oversimplified models of the semiconductor band structure. In such models, the crystal properties are characterized by three parameters, namely, the band gap, the phonon frequency, and the ratio of the rate of phonon emission to that of impact ionization. The price of this oversimplification had been that correspondence with experiment could be achieved only by assuming unphysically large rates of phonon losses (about 0.5 eV per created e-h pair). This does not corroborate with the known values for the ratio of the impact ionization and the phonon emission probabilities for high-energy electrons in semiconductors. The model furthermore obscures the role of features in the band structure and the ionization process that are specific to a particular semiconductor.

In order to elucidate semiconductor-specific issues of the PEB process, we have undertaken theoretical studies of various extensions of the RSA model. Firstly, we studied a model of particles that expand or shrink upon adsorption [19]. The shrinking model is relevant to the PEB problem in that it helps to elucidate such factors as the non-constant density of states in the semiconductor band and the fact that due to momentum conservation the ionization threshold is larger than the bandgap energy that is actually lost in impact ionization.

Subsequently [20], we extended the RSA model in a different direction — competitive deposition of different-size particles from a binary mixture — suitable to simulate the role of multiple channels of pair production, owing to the *multi-valley nature of semiconductor bands*. The interplay between different channels has never been properly addressed but we have found it to be crucial for understanding of the PEB statistics.

In Si, Ge and common A_3B_5 semiconductors, such as InP and GaAs, the e-h pair creation produces electrons in one of the ellipsoids near the edge of the Brillouin zone, in 100 (X) or 111 (L) directions. Owing to the difference in the final densities of states and the matrix elements, the impact ionization processes associated with X and L valleys have different but competitive probabilities. Because of its low density of states, the Γ valley is usually not competitive, even when it is the lowest valley, and in first approximation the probability of electron generation in the Γ-valley can be neglected. This means that the branching competition occurs only between the X and L valleys.

Ultimately, electrons will end up in the lowest energy valley but when that valley is itself degenerate, as in Ge or Si, the final electron states may not be fully equivalent, because of the different collection kinetics due to crystal anisotropy. In *direct-gap* semiconductors, like InP and GaAs, the lowest (Γ) electron valley is non-competitive. In the competitive satellite X and L valleys both the density of states and the threshold energy are different. Our binary-mixture RSA model interprets the higher density of states as higher deposition rate and the higher threshold as larger particle size. We found that the presence of competing channels with different energies will decrease the yield and enlarge the Fano factor. The attendant loss in energy resolution is small when the ionization energies

associated with different valleys are not too disparate. For example, in Ge besides the 8 lowest L valleys (E_G = 0.66 eV) one has a non-competitive Γ-valley (E_Γ = 0.8 eV) and 6 very competitive Si-like valleys (E_G =0.85 eV). The energy resolution downgrading should be more important for crystals with larger (≈2) threshold energy ratio. For example, in Si one has besides the 6 lowest valleys (E_G = 1.12 eV) in X direction, 8 Ge-like L valleys with the gap E_L =2.0 eV. Their effect on the Fano factor in silicon may not be negligible.

The most important effect we found [20] is a very strong *anti-correlation* between competing fluctuations in different valleys. It is particularly evident when one considers *similar* competing valleys, e.g. parking of cars that are different only in "color". Even though the choice of valley is truly random, the total number of cars (symmetric with respect to color) is fully constrained by Fano correlations. This constrain suppresses fluctuations of the total particle number compared to those of partial contributions by different valleys, cf. Fig. 5. This effect may have dramatic consequences for the observed variance, if the symmetry between anti-correlated valleys is broken by a biased collection.

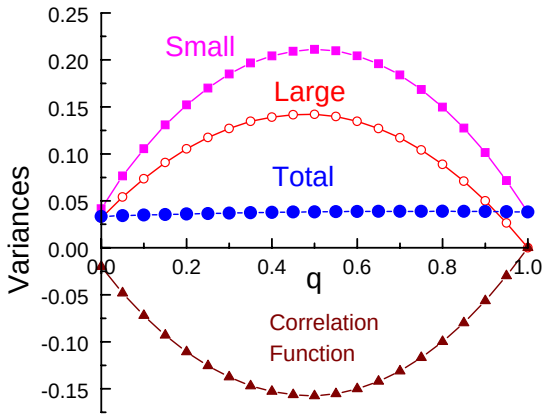

Fig. 5. Fluctuations in random sequential adsorption from a binary mixture [20].

Plotted are the variances of the partial number of adsorbed small (n_a) and large (n_b) particles as functions of the ratio q of small particles in the flux for particle size ratio b/a = 1.2. Also plotted is the correlation function (per unit length x of the "parking lot"):

$$f_{corr} = x^{-1}\langle \delta n_a \delta n_b \rangle$$

For example, in Si diode detectors electrons are created in 6 degenerate energy valleys that represent ellipsoids of revolution elongated along (100) and equivalent ***k***-space directions. The diode are usually designed so that the current flows along the (100) direction. Electrons from the two valleys along the current have a large mass and low mobility. The measured current is hence dominated by electrons from the 4 valleys elongated perpendicular to the current that have a low mass and high mobility along the current. Since the choice of equivalent valley in the PEB process is fully random, the number of high-mobility electrons will fluctuate more strongly than the total number of carriers.

Any collection disparity breaks the symmetry between the equivalent valleys and destroys this anti-correlation. In germanium diodes all different valleys are equivalent relative to the (100) direction and the symmetry is not broken. It would be broken, however, if one were to use Ge diodes oriented in (111) direction. The resultant fluctuations will dominate if the inter-valley transition rate is low compared to the inverse collection time.

In the opposite limit, this effect will average out as the collected current will fluctuate in time. The current fluctuation mechanism due to the carrier escape into heavy-mass valleys is a well-known source of noise in multi-valley semiconductors [21].

We have arrived [20] at a number of qualitative conclusions that should be taken into account in both the interpretation of experimental data and the choice of the crystal composition and device structure in gamma detectors optimized for energy resolution. We plan to address these and similar issues quantitatively for semiconductors of interest. In the context of the present proposal, we shall carry out a detailed theoretical study of variance in 3D-pixellated InP and GaAs γ-detector in comparison with that in Si, Ge, and CZT diodes.

The proposed theoretical study of radiation detector statistics will begin by studies of the multi-channel electro-hole pair generation processes, using analytical as well as numerical (Monte Carlo) techniques. The study will take into account realistic energy distribution between the secondaries, as implied by the impact ionization cross-section, and the smearing of the ionization threshold by phonon emission. Our aim is a reliable theoretical prediction of the performance of InP and GaAs detectors in isotope discrimination.

Other aspects of the proposed statistical studies include the fluctuations associated with the spatial distribution of sources of scintillating radiation within 3D pixels, the effect of inhomogeneity of the heavily doped material on the recycling of scintillating photons and the effect of boundary conditions on pixel surfaces. Other random processes that we shall investigate include incomplete energy conversion and partial delivery of scintillating radiation to the photodiode.

References Cited

[1] G.F. Knoll, *Radiation Detection and Measurement*, 3rd edition, John Wiley & Sons, Inc. (2000).

[2] A. Kastalsky, S. Luryi, B. Spivak, "Semiconductor high-energy radiation scintillation detector", *Nucl. Instr. Meth. Phys. Res*. **A 565**, pp. 650-656 (2006).

[3] A. Kastalsky, S. Luryi, B. Spivak, US Patent Application *Ser. No. 11/144,443*, "Semiconductor scintillation high-energy radiation detector", filed 06/06/2005.

[4] A. Kastalsky and S. Luryi, US Pat. Application *Ser. No. 11/703,805* "High-energy scintillation detector comprising multiple semiconductor slabs", filed 02/08/2007.

[5] W.P. Dumke, M.R. Lorenz, G.D. Pettit, "Intra- and Interband Free-carrier Absorption and the Fundamental Absorption Edge in *n*-Type InP", *Phys. Rev.* **B1**, pp. 4668-4673 (1970).

[6] F. K. Reinhart, "Direct determination of the free-carrier injection density, the free-carrier absorption, and the recombination factors in double heterostructure diodes by optical phase measurements", *J. Appl. Phys.* **97**, pp. 123536:1-13 (2005).

[7] R. E. Nahory, M. A. Pollack, W. D. Johnston, R. L. Barns, "Bandgap versus composition and demonstration of Vegard's law for InGaAsP lattice-matched to InP", *Appl. Phys. Lett.* **33**, pp. 659-661 (1978).

[8] M. Henini, Editor, "*Dilute Nitrides Semiconductors*", Elsevier (2005).

[9] M. Reason, H.A. McKay, B. Nickels, D. Mao, X. Bai, C. Kurdak, R.S. Goldman, "Optimization of GaAsN Electron Mobility", preprint (2006).

[10] F. Zhang, Z. He, G. F. Knoll, D. K. Wehe, J. E. Berry, "3-D Position Sensitive CdZnTe Spectrometer Performance Using Third Generation VAS/TAT Readout Electronics", *IEEE Trans. Nucl. Sci.* **52**, pp. 2009-2016 (2005).

[11] J.D. Kurfess, W.N. Johnson, R.A. Kroeger, B.F. Phlips, "Considerations for the next Compton Telescope Mission", *5th Compton Symp.*, Portsmouth, NH (1999).

[12] S.E. Boggs and P. Jean, "Event reconstruction in high resolution Compton telescopes", *Astron. Astrophys. Suppl. Ser.* **145**, pp. 311-321 (2000).

[13] E. Aprile, A. Bolotnikov, D. Chen, R. Mukherjee, "A Monte Carlo analysis of the liquid xenon TPC as gamma-ray telescope", *Nucl. Inst. Meth. Phys. Res*. **A 327**, pp. 216-221 (1993).

[14] G. Bertuccio, A. Pullia, J. Lauter, A. Forster, H. Luth, "Pixel X-ray detectors in epitaxial gallium arsenide with high-energy resolution capabilities", *IEEE Trans. Nucl. Sci.* **44**, pp. 1-5 (1997).

[15] H. Morkoç, "Comprehensive characterization of hydride VPE grown GaN layers and templates", *Mat. Sci. and Eng.* **R33**, pp. 135-207 (2001).

[16] This correlation originates from the basic fact that a simple random division of a segment in two parts produces highly correlated pieces: if one is short the other is long and vice versa. Energy branching by impact ionization evidently has the similar property, as the sum of secondary-particle energies is fixed by energy conservation. This type of correlations was first pointed out by Ugo Fano in 1947 [U. Fano, "Ionization Yield of Radiations. II. The Fluctuations of the Number of Ions," *Phys. Rev*. **72**, pp. 26-29 (1947)] and bears his name.

[17] W. van Roosbroeck, "Theory of the Yield and Fano Factor of Electron-Hole Pairs Generated in Semiconductors by High-Energy Particles," *Phys. Rev.* **139**, pp. A1702-A1716 (1965).

[18] G.D. Alkhazov, A.A. Vorob'ev, A.P. Komar, "Ionization fluctuations and resolution of ionization chambers and semiconductor detectors," *Nucl. Instr. Meth.* **48**, pp. 1-12 (1967).

[19] A. V. Subashiev and S. Luryi, "Random sequential adsorption of shrinking or expanding particles," *Phys. Rev*. **E 75**, 011123, pp. 1-10 (2007).

[20] A. V. Subashiev and S. Luryi, "Fluctuations of the partial filling factors in competitive RSA from binary mixtures," *Phys. Rev.* **E76** (July 2007); [ArXiv: cond-mat/0704.1235].

[21] Sh. Kogan, *Electronic Noise and Fluctuations in Solids*, Cambridge University Press, Cambridge (1996).

[22] H.B. Barber, B.A. Apotovsky, F.L. Augustine, H.H. Barrett, E.L. Dereniak, F.P. Doty, J.D. Eskin, W.J. Hamilton, D.G. Marks, K.J. Matherson, J.E. Venzon, J.M. Woolfenden, E.T. Young, "Semiconductor pixel detectors for gamma-ray imaging in nuclear medicine," *Nucl. Inst. Meth. Phys. Res*. **A 395**, pp. 421-428 (1997).